Dynamic simulations of membranes with cytoskeletal interactions

Lawrence C.-L. Lin

Department of Physics, University of California, Santa Barbara, California 93106-9530, USA

Frank L. H. Brown

Department of Chemistry and Biochemistry, University of California, Santa Barbara, California 93106-9510, USA

We describe a simulation algorithm for the dynamics of elastic membrane sheets over long length and time scales. Our model includes implicit hydrodynamic coupling between membrane and surrounding solvent and allows for arbitrary external forces acting on the membrane surface. In particular, the methodology is well suited to studying membranes in interaction with cytoskeletal filaments. We present results for the thermal undulations of a lipid bilayer attached to a regular network of spectrin filaments as a model for the red blood cell membrane. The dynamic fluctuations of the bilayer over the spectrin network are quantified and used to predict the macroscopic diffusion constant of band 3 on the surface of the red blood cell. We find that thermal undulations likely play a role in the mobility of band 3 in the plane of the erythrocyte membrane.

PACS number(s): 87.16.Ac, 87.15.Vv, 87.16.Dg, 83.10.Mj

INTRODUCTION

Biological membranes are fundamental to a vast number of biophysical processes. Of the various computational techniques that have been developed to study lipid bilayer membranes, fully atomistic simulations containing both lipid and solvent molecules [1–5] are the most realistic, but are subject to computational constraints. As a result, such simulations are currently only able to achieve length and time scales on the order of tens of nanometers and tens of nanoseconds, respectively. Since many biological processes occur over scales orders of magnitude larger, the phenomena that can be studied at this level of detail are quite restricted. Many models have been developed to extend the distances and times over which membrane-dependent processes can be simulated. These models usually contain simplified lipids and water molecules [6–13]. Less commonly, solvent may be treated implicitly [14–17]. Although these methods are promising, they remain under development. Widespread use of simplified particle based models for membrane systems has yet to become a reality.

Theoretical treatments of the lipid bilayer have thus far been the only means for quantitative analysis of processes that occur on the longest biologically relevant length and time scales. An elastic model for fluid membrane sheets developed by Helfrich [18] has been successfully applied to many different biophysical problems such as the flicker effect in red blood cells [19], the interaction between membrane-bound proteins [20–24], and the formation of the immunological synapse [25]. Overdamped thermal membrane dynamics are captured within this framework via stochastic coupling between the membrane sheet and an implicit solvent environment [19,26–29]. Interactions beyond the coupling between membrane and solvent (e.g., cytoskeletal attachments, extracellular matrices, experimentally applied forces, etc.) are only analytically tractable for harmonic perturbations in sufficiently simple geometries [30–33]. General anharmonic interactions have been studied computationally via Monte Carlo simulation [34–36], but only in the context of thermal (time-independent) averages.

In a recent letter, we introduced a Fourier Space Brownian Dynamics (FSBD) simulation method [37] capable of studying dynamics of lipid bilayers subject to anharmonic perturbations. The method was shown to be capable of simulating membrane dynamics out to long length scales (microns) and slow time scales (seconds), making studies of certain cellular-scale biophysical phenomena feasible. In part, the methodology component of this paper is a detailed account of the work introduced in our preliminary report. Additionally, the present work extends our previous treatment to systems with nonvanishing surface tensions. The application component of this paper fully discusses our work on the diffusion of band 3 protein on red blood cell membranes. These results were briefly quoted in the letter version of this work without significant analysis or discussion of results.

The motion of band 3 protein on the red blood cell (RBC) membrane surface is known to deviate [38–42] from the purely diffusive behavior predicted by the fluid mosaic model [43,44]. The motion of the protein exhibits one diffusion constant on small length scales and a smaller diffusion constant over length scales longer than hundreds of nanometers [45–51]. This behavior is known to be a result of the steric interaction between the protein and the underlying network of corrals formed by the spectrin cytoskeleton [42,52] as illustrated in Fig. 1.

Although it is clear that the cytoskeleton plays a role in protein mobility, the mechanism by which the protein escapes the corrals is not well established. Previous theoretical studies have used simple, nonspecific potential barriers at the corral boundary [53] or have assumed that rearrangements of the spectrin network are necessary for a protein to escape confinement [54–58]. In recent work [29,33], we have alternatively proposed that thermal fluctuations of the membrane may help promote the passage of band 3 by lifting it over the cytoskeletal barrier. The models that have been studied in this context include a free membrane [29] and a membrane with localized harmonic pinning between the cytoskeleton and bilayer [33]. In both prior studies, however, we were
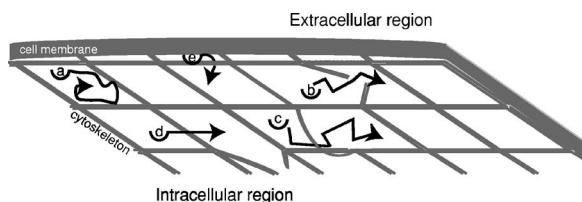
FIG. 1. Schematic illustration of the behavior of transmembrane proteins in the red blood cell. The cytoskeleton immediately below the membrane hinders protein transport by confining the protein temporarily to a localized corral (a). Jumps from one corral to another occur slowly and have previously been postulated to result from dynamic reorganization of the cytoskeletal matrix, either by dissociation of spectrin tetramers (b) or thermal fluctuations in the shape of the cytoskeleton (c), or by infrequent crossing events where the protein is thermally kicked hard enough to force its way over a relatively static cytoskeleton (d). The present study considers the alternative possibility that shape fluctuations of the lipid bilayer may allow for corral hopping (e). This possibility has been previously investigated [29,33] using models that did not properly account for interactions between spectrin and membrane. The present work is able to model such interactions explicitly via the Fourier space Brownian dynamics simulation algorithm.

forced to neglect the nonharmonic repulsive interaction between membrane and spectrin filaments since our previous computational methods were restricted to harmonic models. The FSBD algorithm is applicable to anharmonic models and allows us to model this repulsion explicitly. We find, in qualitative agreement with previous models, that thermal fluctuations should play a role in protein mobility on the surface of the red blood cell. Quantitatively, the results of the present study are in better agreement with experiment than previously obtained.

This paper is organized as follows. First, we discuss our model of protein mobility and quantify the macroscopic diffusivity of band 3 on the RBC in terms of a dynamic gating mechanism regulated by thermal undulations of the lipid bilayer above spectrin filaments. We then introduce the equations that specify the dynamics of the lipid bilayer and present the FSBD simulation methodology in detail. Several applications of our algorithm follow in the next two sections. We first consider a number of analytically tractable harmonic systems and compute correlation functions as well as quantities related to the problem of protein mobility. In these cases, comparisons between exact results and simulation are possible and the FSBD algorithm is shown to be robust. For nonharmonic systems, the only previously obtained results are equilibrium averages from Monte Carlo simulations. We verify FSBD in this case for a model of a stack interacting membranes first studied by Gouliaev and Nagle [34]. Having established the accuracy of FSBD, we return to the problem of RBC protein mobility and improve upon previous harmonic models by adding anharmonic repulsive interactions between spectrin and the bilayer. This model for the RBC membrane is simulated using FSBD leading to mobility estimates for band 3 protein moving in a realistic environment at the red blood cell surface. Finally, we discuss the results and conclude.

PROTEIN MOBILITY

We develop a model of protein mobility on the surface of the red blood cell that depends on thermal fluctuations of the membrane as the mechanism governing the rate of diffusion. As discussed in the introduction, the structure of the cytoskeleton plays an important role in the mobility of band 3 in the plane of the bilayer. Electron microscopy shows a series of roughly triangular corrals formed by spectrin filaments [59,60] that connect to the membrane by various proteins at discrete locations [61–64]. Free diffusive motion occurs within the corrals on length scales of tens of nanometers. However, on longer length scales, the spectrin cytoskeleton hinders the motion of the protein, although occasional hopping between corrals is observed [51]. Various theories, discussed in the introduction and illustrated in Fig. 1, have been proposed to explain how the protein escapes local confinement. Although many of these mechanisms likely contribute to the macroscopic diffusivity, we focus on the role of thermal membrane undulations as a means for aiding the passage of band 3 over the cytoskeletal barrier.

We use the same framework to describe the diffusion of the protein as in previous work [29,33]. Experimentally, the microscopic diffusion constant for band 3 within a corral D =0.53 $\mu\text{m}^2\,\text{s}^{-1}$ is observed to be two orders of magnitude larger than the macroscopic diffusion constant D_{macro}=6.6 $\times 10^{-3}$ $\mu\text{m}^2\,\text{s}^{-1}$ [51], a fact attributed to the hindering of the protein by the cytoskeleton (see Fig. 1). We assume that the protein cannot escape the corral unless the local height of the membrane along the border of the corral exceeds the height $h_0 \sim 6$ nm [65] of the cytoplasmic domain of the protein. At smaller separations between bilayer and spectrin, the protein will collide with spectrin in any attempt to escape a corral. Within our picture, thermal fluctuations of the membrane provide the means by which the protein can be lifted over the cytoskeletal barrier.

Since the protein cannot instantaneously diffuse over spectrin, we also require that the height fluctuation greater than h_0 persist for a time of at least t_D to allow diffusive passage to occur. An estimate for this time scale is obtained by assuming that the protein needs to diffuse a distance ℓ =7 nm (half the width of band 3 plus half of the width of the spectrin) [57] in order to get over the cytoskeleton. The time it takes the protein to diffuse this distance is based on the value of the microscopic diffusion constant and approximated to be $t_D = \ell^2/4D = 23$ μs.

In our model, membrane shape is specified by a local height $h(\mathbf{r})$ as a function of the position $\mathbf{r} = (x,y)$ in the xy plane. This representation is called the Monge gauge [66] and is chosen for several reasons. Given that we are interested in length scales (on the order of ~ 100 nm) much smaller than the size of the closed, biconcave-shaped red blood cell (~ 7 μm), the curvature of the surface can be neglected and the membrane is essentially specified by the $h(\mathbf{r})=0$ plane in the absence of stochastic forces. Later, we show quantitatively that the thermal undulations away from this reference plane are small so that we can neglect forces in the xy plane and focus only on height fluctuations in the z direction. The above considerations make the Monge parametrization a logical choice for describing the local height of

the membrane due to random thermal fluctuations.

We now quantify the probability that the protein escapes through the edge of the corral. Since we deny the passage of band 3 unless the height of the membrane $h(\mathbf{r})$ exceeds h_0, we define the equilibrium probability that $h(\mathbf{r}) > h_0$ as

$$P(\mathbf{r}) = \langle \Theta(h(\mathbf{r}) - h_0) \rangle, \qquad (1)$$

where Θ is the Heaviside step function. We also require that the gap is open for a long enough time period for the protein to diffuse out of the corral. An approximate way to quantify this condition uses the correlated probability that $h(\mathbf{r}) > h_0$ at time t given that $h(\mathbf{r}) > h_0$ at time 0

$$C(\mathbf{r},t) = \frac{\langle \Theta(h(\mathbf{r},t) - h_0) \Theta(h(\mathbf{r},0) - h_0) \rangle - P^2(\mathbf{r})}{P(\mathbf{r}) - P^2(\mathbf{r})}. \qquad (2)$$

We have subtracted off the random, uncorrelated probability that $h(\mathbf{r}) > h_0$ at times 0 and t. For more details, see Appendix C in Lin and Brown [33]. The product $P(\mathbf{r})C(\mathbf{r},t_D)$ reflects the approximate probability that a gap of size h_0 will open for a time t_D. Note that the cytoskeletal barriers at the edges are fixed at height zero and taken to be static. We choose to neglect spectrin dynamics, which has been studied elsewhere (as discussed in the introduction), and focus on the effect of membrane fluctuations.

A simple model of the diffusion of the protein leads to a macroscopic diffusion constant. From this point forward, we define L as the length of one side of the corral taken to be roughly $L \sim 110$ nm to agree with experiment [51]. We will later study both square and triangular corrals. The probability that the gap is large enough for the duration of the required time t_D averaged over one edge of the corral is

$$Q(t_D) \equiv \frac{1}{L} \int_0^L dx\, P(x)C(x,t_D). \qquad (3)$$

Within a square corral, the protein executes a random walk on a square lattice with spacing $\ell = 7$ nm. The protein has probability Q of escaping if it happens to be on the corral edge and moving in the proper direction to escape. Using this model, a macroscopic diffusion constant is obtained for the geometry of a square grid [33]

$$D_{\text{macro}} = \frac{k_{\text{sq}}L^2}{4}, \qquad (4)$$

where $k_{\text{sq}} = f_{\text{sq}}Q_{\text{sq}}(t_D)/4t_D$ is the escape rate, and $f_{\text{sq}} = (4N_{\text{sq}} - 4)/N_{\text{sq}}^2$ is the probability of being on a boundary square, and $N_{\text{sq}} = L/\ell$ is the number of lattice points on the boundary. For the triangular geometry, the diffusion occurs between the centers of equilateral triangles with sides length $2\ell\sqrt{3}$ so that the random walk is on a hexagonal lattice with steps length ℓ. The diffusion constant is [33]

$$D_{\text{macro}} = \frac{3k_{\text{tr}}L^2}{16}, \qquad (5)$$

where $k_{\text{tri}} = f_{\text{tri}}Q_{\text{tri}}(t_D)/3t_D$, $f_{\text{tri}} = (3N_{\text{tri}} - 3)/N_{\text{tri}}^2$, and $N_{\text{tri}} = \sqrt{3}L/2\ell$. Our simulations provide explicit data for $P(\mathbf{r})$ and $C(\mathbf{r},t)$. Macroscopic diffusion constants follow immediately from these quantities via Eqs. (4) and (5).

THEORY OF MEMBRANE DYNAMICS

Our starting point is the elastic energy for a fluid quasiplanar sheet [18,66] in the presence of external perturbations

$$H = \int_{\mathcal{A}} d\mathbf{r} \left(\frac{K_c}{2}[\nabla^2 h(\mathbf{r})]^2 + \frac{\sigma}{2}[\nabla h(\mathbf{r})]^2 \right) + H_{\text{int}}[h(\mathbf{r})], \quad (6)$$

where K_c is the bending modulus, σ is the surface tension, and $\mathcal{A} = \mathcal{L}^2$ is the projected area of a square patch of membrane. As noted in the preceding section, the membrane is parametrized by the height $h(\mathbf{r})$ where $\mathbf{r} = (x,y)$ is the position in the xy plane. The system is taken to be periodic with period $\mathcal{L}$ in both x and y. The elastic model specified by Eq. (6) is applicable down to wavelengths of ~ 3–6 nm [67–69]. Finer spatial resolution in the xy plane would require treatment of molecular level detail, however the mesoscopic questions addressed in the present work naturally suggest a coarse graining scale larger than 6 nm.

The first term of H in Eq. (6) is an elastic energy related to the mean curvature of the membrane and the second term is a surface tension energy related to the total area of the membrane. Both are approximations in the limit of small fluctuations $[|\nabla h(\mathbf{r})| \ll 1]$ which we show later to be the appropriate regime for the systems we study. The term $H_{\text{int}}[h(\mathbf{r})]$ allows for interactions between the membrane and its surroundings and is allowed to be an arbitrary functional of the height $h(\mathbf{r})$. For our purposes, we require only local interactions and define a density $\mathcal{H}_{\text{int}}(h(\mathbf{r}))$ through

$$H_{\text{int}}[h(\mathbf{r})] = \int_{\mathcal{A}} d\mathbf{r}\, \mathcal{H}_{\text{int}}(h(\mathbf{r})). \qquad (7)$$

More general forms such as

$$\int_{\mathcal{A}} d\mathbf{r} \int_{\mathcal{A}} d\mathbf{r}' \mathcal{H}_{\text{int}}(h(\mathbf{r}),h(\mathbf{r}')) \qquad (8)$$

or higher orders in a functional expansion are certainly possible and relevant in the case of other biophysical problems, but not necessary in the context of the present study.

The dynamics of the system are specified by starting with the Navier-Stokes equations for a set of interacting particles in an incompressible fluid. In the low Reynolds number regime, which we show later to apply to the red blood cell, inertia can be neglected and the equation for the velocities of each particle can be obtained [70]. Taking the continuum limit and adding a random force, the stochastic dynamics of the bilayer are described by a nonlocal Langevin equation [28]

$$\frac{\partial h(\mathbf{r},t)}{\partial t} = \int_{-\infty}^{\infty} d\mathbf{r}' \Lambda(\mathbf{r} - \mathbf{r}')[F(\mathbf{r}',t) + \zeta(\mathbf{r}',t)], \qquad (9)$$

where $\Lambda(\mathbf{r} - \mathbf{r}') = 1/8\pi\eta|\mathbf{r} - \mathbf{r}'|$ is the diagonal part of the Oseen tensor, η is the viscosity of the surrounding fluid, $F(\mathbf{r},t) = -\delta H/\delta h(\mathbf{r},t)$ is the force per unit area on the membrane, and $\zeta(\mathbf{r},t)$ is a Gaussian white noise satisfying the fluctuation-dissipation relation [70]

TABLE I. Model parameters, the surface tension σ is negligible under physiological conditions, but we have taken nonzero values in several examples for purposes of illustration.

Parameter	Description	Value	Reference
K_c	Bending modulus	2×10^{-13} ergs	[a]
η	Cytoplasm viscosity	0.06 poise	[a]
T	Temperature	37 °C	Body temperature
h_0	Depth of cytoplasmic domain of band 3	6 nm	[b]
D	Band 3 diffusion constant	0.53 μm^2 s^{-1}	[c]
ℓ	Lattice spacing	7 nm	[d]
t_D	Random walk time step	23 μs	[d]
γ	Pinning constant	2.0×10^{14} ergs cm^{-4}	
ϵ	Repulsive potential energy scale	8.7×10^{-4} ergs cm^{-2}	
λ	Repulsive potential length scale	0.2 nm	[e]

[a]Brochard and Lennon [19].
[b]Zhang *et al.* [65].
[c]Tomishige *et al.* [51].
[d]Brown [29].
[e]Podgornik and Parsegian [73].

$$\langle \zeta(\mathbf{r},t) \rangle = 0, \tag{10}$$

$$\langle \zeta(\mathbf{r},t) \zeta(\mathbf{r}',t') \rangle = 2k_B T \Lambda^{-1}(\mathbf{r} - \mathbf{r}') \delta(t - t'), \tag{?}$$

where the inverse of $\Lambda(\mathbf{r} - \mathbf{r}')$ is defined by

$$\int_{-\infty}^{\infty} d\mathbf{r}' \Lambda(\mathbf{r} - \mathbf{r}') \Lambda^{-1}(\mathbf{r}') = \delta(\mathbf{r}). \tag{11}$$

The force per unit area in our case is

$$F(\mathbf{r},t) = -K_c \nabla^4 h(\mathbf{r}) + \sigma \nabla^2 h(\mathbf{r}) - \frac{\partial \mathcal{H}_{\text{int}}(h(\mathbf{r}))}{\partial h(\mathbf{r})}. \tag{12}$$

These equations completely specify the dynamics of the lipid bilayer.

The most computationally efficient way to handle Eq. (9) is to convert to Fourier space using

$$h_{\mathbf{k}} = \int_{\mathcal{A}} d\mathbf{r}\, h(\mathbf{r}) e^{-i\mathbf{k}\cdot\mathbf{r}}, \tag{13}$$

$$h(\mathbf{r}) = \frac{1}{\mathcal{L}^2} \sum_{\mathbf{k}} h_{\mathbf{k}} e^{i\mathbf{k}\cdot\mathbf{r}}. \tag{14}$$

The equation of motion for each mode becomes

$$\frac{\partial h_{\mathbf{k}}(t)}{\partial t} = \Lambda_{\mathbf{k}} \{ F_{\mathbf{k}}[h(\mathbf{r},t)] + \zeta_{\mathbf{k}}(t) \}, \tag{15}$$

where $\Lambda_{\mathbf{k}} = 1/4\eta k$, and $\zeta_{\mathbf{k}}(t)$ now obeys

$$\langle \zeta_{\mathbf{k}}(t) \rangle = 0, \tag{16}$$

$$\langle \zeta_{\mathbf{k}}(t) \zeta_{\mathbf{k}'}(t') \rangle = 2k_B T \mathcal{L}^2 \Lambda_{\mathbf{k}}^{-1} \delta_{\mathbf{k},-\mathbf{k}'} \delta(t - t'). \tag{17}$$

The values of the wave vectors are those consistent with the periodic boundary conditions $\mathbf{k} = (m,n) 2\pi/\mathcal{L}$ and a short

wavelength cutoff is imposed by the restriction $-N/2 < m, n \leq N/2$ where $N = \mathcal{L}/\ell$. For general potentials, the Fourier transform of the force $F_{\mathbf{k}}$ depends on the entire set $\{h_{\mathbf{k}}\}$ making Eq. (15) a set of coupled equations. However, for the free membrane ($H_{\text{int}} = 0$), we obtain $F_{\mathbf{k}} = -(K_c k^4 + \sigma k^2) h_{\mathbf{k}}$ and the equations decouple

$$H = \frac{1}{2\mathcal{L}^2} \sum_{\mathbf{k}} (K_c k^4 + \sigma k^2) |h_{\mathbf{k}}|^2, \tag{18}$$

$$\dot{h}_{\mathbf{k}} = -\left(\frac{K_c k^4 + \sigma k^2}{4\eta k} \right) h_{\mathbf{k}} + \Lambda_{\mathbf{k}} \zeta_{\mathbf{k}} \tag{19}$$

making the Fourier representation a natural basis for membrane dynamics in the absence of interactions. In general cases, the Fourier basis is preferable to real space approaches for its natural handling of hydrodynamic effects without the convolution of Eq. (9).

We now show that the assumption of small fluctuations is self-consistent for the case of the free membrane. From the equipartition theorem, the mean square amplitude of $h_{\mathbf{k}}$ is

$$\langle |h_{\mathbf{k}}|^2 \rangle = \frac{k_B T \mathcal{L}^2}{K_c k^4 + \sigma k^2} \tag{20}$$

which gives for the excitation of a single mode $h_{\mathbf{k}}$ the mean square displacement

$$\langle h^2(\mathbf{r}) \rangle \sim \frac{1}{\mathcal{L}^4} \langle |h_{\mathbf{k}}|^2 \rangle \sim \frac{k_B T}{\mathcal{L}^2 (K_c k^4 + \sigma k^2)}. \tag{21}$$

Picking out the dominant contribution, we use for the value of k the longest wavelength mode $2\pi/\mathcal{L}$. Using the physical parameters for the red blood cell in Table I along with the fact that we are concerned with system sizes $\mathcal{L}$ on the order of hundreds of nanometers, the resulting average height of the membrane is only several nanometers. We conclude that

we are safely in the regime of small fluctuations with $|\nabla h(\mathbf{r})| \ll 1$.

We can also justify the assumption of low Reynolds number in the absence of interactions. Given a particular $\mathbf{k}$ mode, we establish a characteristic length $d \sim 2\pi/k$, and a characteristic velocity

$$u = \frac{1}{\mathcal{L}^2}\dot{h}_{\mathbf{k}} = \frac{1}{\mathcal{L}^2}\Lambda_{\mathbf{k}}F_{\mathbf{k}} = \frac{1}{\mathcal{L}^2}\frac{K_c k^4 + \sigma k^2}{4\eta k}h_{\mathbf{k}}. \qquad (22)$$

Using the root mean square average in place of the amplitude $h_{\mathbf{k}}$, the Reynolds number is approximated by

$$\text{Re} = \frac{ud\rho}{\eta} \sim \frac{\rho}{\eta^2 \mathcal{L}}\sqrt{k_B T\left(K_c + \frac{\sigma}{k^2}\right)}. \qquad (23)$$

Using the constants in Table I, we obtain $\text{Re} \sim 10^{-6}$ which justifies our neglect of inertia in the hydrodynamic equations.

The $\mathbf{k}=0$ mode, related to the center of mass of the system $h_{\text{c.m.}} \equiv h_{\mathbf{k}=0}/\mathcal{L}^2$, presents a unique complication. In Eq. (9), the velocity depends on a sum of hydrodynamic contributions over all space, including periodic copies. For the $\mathbf{k}=0$ mode, the $1/r$ form of the Oseen interaction leads to a divergence in $\Lambda_{\mathbf{k}} = 1/4\eta k$. For systems that have a fixed center of mass, we simply set $\Lambda_{\mathbf{k}=0}$ to zero and the problem is avoided. For systems where this constraint is unnatural, we use the value for the diffusion of a membrane of area $\mathcal{A}$ given by $\Lambda_0 \simeq 3\mathcal{L}/8\pi\eta$ [33]. It is clear that this choice affects the dynamics of the system in most situations. However, we always consider a specific limit in which the results become independent of Λ_0. We now show that in the presence of a confining potential and in the limit of large system sizes, the variance of $h_{\text{c.m.}}$ goes to zero. In this case, the center of mass is essentially fixed to its equilibrium value $\langle h_{\mathbf{k}=0}\rangle$ and the motion of the center of mass vanishes. In this limit, the numerical value chosen for $\Lambda_{\mathbf{k}=0}$ is irrelevant, provided a large enough value is chosen to ensure relaxation to equilibrium over simulation time scales. To prove this hypothesis, consider the addition of a harmonic uniform confining potential

$$H_{\text{int}}[h(\mathbf{r})] = \gamma \int_{\mathcal{A}} d\mathbf{r}\, h^2(\mathbf{r}) \qquad (24)$$

to the free membrane Hamiltonian. The variance in the center of mass for this harmonically bound membrane is

$$\langle h_{\text{c.m.}}^2\rangle - \langle h_{\text{c.m.}}\rangle^2 = \frac{k_B T}{\gamma \mathcal{L}^2} \qquad (25)$$

and vanishes in the limit of large $\mathcal{L}$ as previously asserted.

The systems we consider that require a nonzero center of mass are always studied in the limit of large $\mathcal{L}$. However, they do not have a simple uniform confining potential as above, but rather a periodic set of localized pinning potentials. These pinning interactions fix $h(\mathbf{r})=0$ at specific points of the membrane and are relevant to the case of the red blood cell. The important point is that the membrane center of mass can be thought of as the average height of the membrane. In the presence of a regular confining potential (constant or periodic) there will be some finite correlation length in the xy plane for membrane fluctuations away from $z=\langle h_{\text{c.m.}}\rangle$. For membranes sufficiently larger in linear dimension than this length scale, $h_{\text{c.m.}}$ will reflect an average over independent contributions stemming from patches of membrane separated by more than a correlation length. An average of independent random variables will display a variance that is inversely proportional to the number of independent variables [71]. Consequently, the variance in Eq. (25) is proportional to $1/\mathcal{L}^2$. As $\mathcal{L}$ increases, the number of independent membrane patches increases as the square of $\mathcal{L}$. Although we have displayed this scaling explicitly only for the case of a constant harmonic confining potential, the result is general to more complicated confining interactions. For the pinning potential considered later, we expect our results to be independent of Λ_0 when $\mathcal{L}$ is sufficiently large.

FOURIER SPACE BROWNIAN DYNAMICS (FSBD)

We now present a method of simulating the time evolution of the membrane based on standard Brownian dynamics [72]. Although our equations are of the same form as the traditional method, our dynamical variables are the amplitudes of the Fourier modes. We make this choice largely due to the fact that a fast Fourier transform is computationally more efficient than the convolution in Eq. (9). Additionally, proceeding in Fourier space with a wave-vector cutoff provides a convenient method to coarse grain over microscopic details.

We begin by integrating Eq. (15) from t to $t+\Delta t$ for small Δt,

$$h_{\mathbf{k}}(t+\Delta t) = h_{\mathbf{k}}(t) + \Lambda_{\mathbf{k}}F_{\mathbf{k}}(t)\Delta t + R_{\mathbf{k}}(\Delta t),$$

$$\qquad (26)$$

$$R_{\mathbf{k}}(\Delta t) \equiv \Lambda_{\mathbf{k}}\int_t^{t+\Delta t} dt'\, \zeta_{\mathbf{k}}(t'),$$

where the real and imaginary parts of $R_{\mathbf{k}}(\Delta t)$ are drawn from Gaussian distributions of appropriate width (specified below). A minor complication arises in that $h(\mathbf{r})$ is a real quantity so that the Fourier modes obey $h_{\mathbf{k}}^* = h_{-\mathbf{k}}$. As a result, not all of the amplitudes $h_{\mathbf{k}}$ are independent and only N^2 of the real and imaginary components are evolved in time. Recall that in a discrete Fourier transform, all modes are complex except for four explicitly real modes if N is even, and one explicitly real mode if N is odd. We consider only the case of even N (the method for odd N follows in a straightforward manner). The modes given by $(m,n)=(0,0)$, $(N/2,0)$, $(0,N/2)$, and $(N/2,N/2)$ are completely real and comprise four independent dynamic variables for the system. We choose the other independent modes to be (m,n) for $-N/2 < m < N/2$ and $0 < n < N/2$, $(m,0)$ for $0 < m < N/2$, $(m,N/2)$ for $0 < m < N/2$, and $(N/2,n)$ for $0 < n < N/2$. The remaining modes are complex conjugates of these modes as required by the condition $h_{\mathbf{k}}^* = h_{-\mathbf{k}}$.

The considerations above also apply to the random force $\zeta_{\mathbf{k}} \equiv f_{\mathbf{k}} + ig_{\mathbf{k}}$. From Eq. (16), the fluctuation-dissipation relation for the purely real components is $\langle f_{\mathbf{k}}(t)f_{\mathbf{k}}(t)\rangle = 2k_B T\mathcal{L}^2\Lambda_{\mathbf{k}}^{-1}\delta(t-t')$ while the remaining independent components exhibit $\langle f_{\mathbf{k}}(t)f_{\mathbf{k}}(t)\rangle = \langle g_{\mathbf{k}}(t)g_{\mathbf{k}}(t)\rangle = k_B T\mathcal{L}^2\Lambda_{\mathbf{k}}^{-1}\delta(t-t')$.
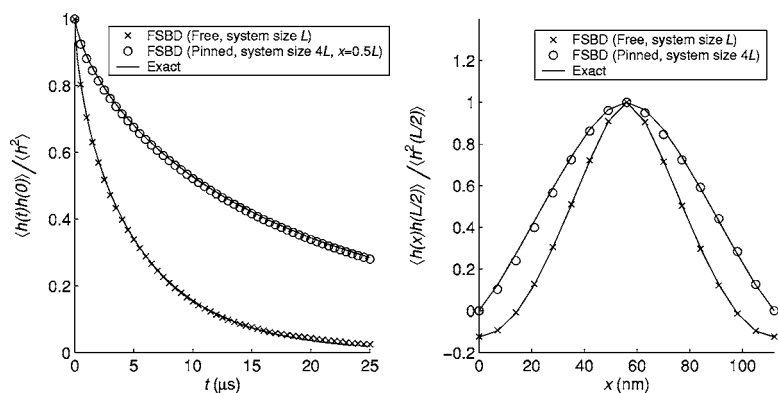
FIG. 2. In the left panel, we plot the normalized time correlation function at the midpoint of the edge of the corral $x=x'=L/2$ for $t'=0$. In the right panel, we plot the correlation in position along the edge of the corral x for fixed $x'=L/2$ and equal times $t=t'$. The averages are computed over all corral edges with length $L=112$ nm. The simulations are done with a time step of $\Delta t = 1$ ns for a total time of $t=0.1$ s using the parameters in Table I. For a discussion of the choice of the time step used, see Appendix B.

Cross correlations between the amplitudes $f_{\mathbf{k}}$ and $g_{\mathbf{k}}$ are all zero. Correspondingly, $R_{\mathbf{k}}(\Delta t)$ is drawn from a Gaussian distribution with zero mean and variance $2\mathcal{L}^2 k_B T \Lambda_{\mathbf{k}} \Delta t$ for the explicitly real modes and the real and imaginary parts of $R_{\mathbf{k}}(\Delta t)$ are drawn from a Gaussian distribution with zero mean and variance $\mathcal{L}^2 k_B T \Lambda_{\mathbf{k}} \Delta t$ for the remaining independent modes.

Simulations proceed from the initial configuration $h(\mathbf{r}) = 0$ for the sheet and evolve according to Eq. (26). Explicitly, a single time step in our Fourier space Brownian dynamics simulation algorithm consists of the following:

(1) Evaluate the interaction part of the forces $F_{\text{int}}(\mathbf{r}) = -\delta H_{\text{int}}/\delta h(\mathbf{r})$ in position space.

(2) Compute the bending forces $F_{\mathbf{k}}^{\text{bend}} = -K_c k^4 h_{\mathbf{k}}$, surface tension forces $F_{\mathbf{k}}^{\text{tens}} = -\sigma k^2 h_{\mathbf{k}}$, and evaluate the interaction force $F_{\mathbf{k}}^{\text{int}}$ by Fourier transforming the result of the previous step.

(3) Draw $R_{\mathbf{k}}(\Delta t)$'s from the Gaussian distributions specified above.

(4) Compute $h_{\mathbf{k}}(t+\Delta t)$ using Eq. (26). Inverse Fourier transformation yields $h(\mathbf{r})$ for use in the next iteration.

In practice, the time step Δt is decreased until our results converge. However, it is possible to estimate the appropriate time step in some simple cases (see Appendix B) to verify that our choices are reasonable. We consider some applications of FSBD in the following sections.

VERIFICATIONS OF FSBD

The free membrane

Models which contain harmonic forms of $\mathcal{H}_{\text{int}}$ can be handled analytically [31–33] and used to verify the accuracy of the FSBD algorithm. The simplest of these is the free membrane for which $\mathcal{H}_{\text{int}}=0$. The exact result for correlations in both time and space is (see Appendix A)

$$\langle h(\mathbf{r},t)h(\mathbf{r}',t')\rangle = \frac{k_B T}{\mathcal{L}^2}\sum_{\mathbf{k}}\frac{e^{-\omega_{\mathbf{k}}|t-t'|}}{K_c k^4 + \sigma k^2}\cos[\mathbf{k}\cdot(\mathbf{r}-\mathbf{r}')],$$

(27)

where the relaxation frequencies are

$$\omega_{\mathbf{k}} = \frac{K_c k^4 + \sigma k^2}{4\eta k}.$$

(28)

We use the expressions above to compare the exact analytical results with those of the FSBD simulation.

For equal positions $\mathbf{r}=\mathbf{r}'$, the normalized height autocorrelation function becomes

$$\frac{\langle h(t)h(0)\rangle}{\langle h^2\rangle} = \frac{\sum_{\mathbf{k}}(K_c k^4 + \sigma k^2)^{-1}e^{-\omega_{\mathbf{k}}t}}{\sum_{\mathbf{k}}(K_c k^4 + \sigma k^2)^{-1}}.$$

(29)

A plot of the exact and FSBD results are shown in Fig. 2 using the parameters for the red blood cell in Table I. We choose our system size to be one corral with $\mathcal{L}=L=112$ nm which is roughly the size of red blood cell corrals [51]. Since the membrane center of mass has equal probability of being anywhere in space, we fix its value to $h_{\text{c.m.}}=0$ as in previous work [29,33]. The membrane is discretized in position space with $\mathcal{L}=N\ell$ and $\ell=7$ nm as described in the section on protein mobility. Also in Fig. 2, we plot the equal-time correlation in position from FSBD along with the analytical expression

$$\frac{\langle h(\mathbf{r})h(\mathbf{r}')\rangle}{\langle h^2\rangle} = \frac{\sum_{\mathbf{k}}(K_c k^4 + \sigma k^2)^{-1}\cos[\mathbf{k}\cdot(\mathbf{r}-\mathbf{r}')]}{\sum_{\mathbf{k}}(K_c k^4 + \sigma k^2)^{-1}}.$$

(30)

The negative correlation near a distance of $L/2$ away from the center is an indication of the dominance of the wavelength L modes.

Under physiological conditions, the bilayer surface tension σ is negligible. However, at length scales exceeding corral dimensions, pinning between bilayer and cytoskeleton leads to a finite effective surface tension for the composite membrane system (bilayer+spectrin) while leaving the shorter wavelength tension zero within experimental uncertainty [74]. We stress this difference between bilayer tension and effective tension of the composite membrane to avoid possible confusion. The effective tension is unimportant to the present work as we are interested in fluctuations affecting a single corral. For convenience, we have chosen a geometry where all pinning sites are coplanar, which translates to an
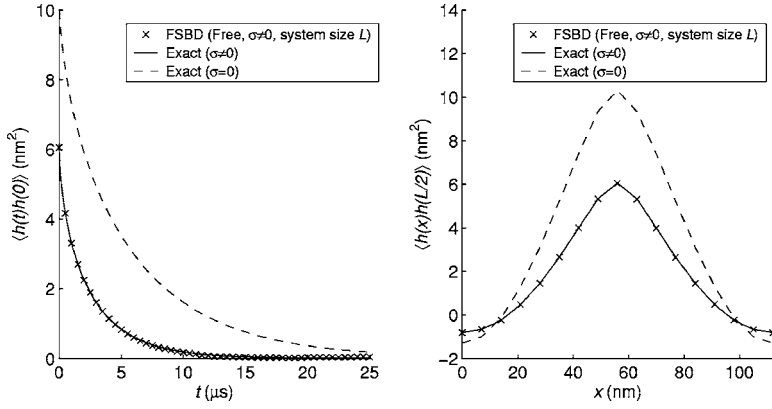
FIG. 3. The same plots as in Fig. 2 except unnormalized and with surface tension $\sigma = (2\pi/\mathcal{L})^2 K_c$. The time correlations fall off more rapidly and height of the undulations is quenched as predicted by Eqs. (29) and (30).

infinitely large long wavelength effective tension. This "tension" does not affect statistics of the fluctuations of interest to us.

To illustrate the effect of a nonzero bilayer surface tension, σ, we choose a value $\sigma = (2\pi/\mathcal{L})^2 K_c$ that cuts the fluctuations of the longest wavelength mode in half as can be seen from Eq. (27). From the relaxation frequencies in Eq. (28), the relaxation time of that mode is half of the zero tension value. Both observations are apparent in Fig. 3 where the unnormalized correlation functions are plotted. The effect of a finite surface tension is to decrease the amplitude of fluctuations and increase their relaxation rate.

Returning to the problem of protein mobility, we calculate the value of the macroscopic diffusion constant for the free membrane. For harmonic models, it is possible to derive analytical expressions for $P(\mathbf{r})$ and $C(\mathbf{r},t)$ in Eqs. (1) and (2). The results are [33]

$$P(\mathbf{r}) = \tfrac{1}{2}\,\mathrm{erfc}[\bar{h}(\mathbf{r})], \qquad (31)$$

where the dimensionless variable $\bar{h}(\mathbf{r})$ is defined as

$$\bar{h}(\mathbf{r}) \equiv \frac{h_0}{\sqrt{2\langle h^2(\mathbf{r})\rangle}}, \qquad (32)$$

and

$$C(\mathbf{r},t) = \frac{1}{P(\mathbf{r}) - P^2(\mathbf{r})}\left[\frac{1}{2\sqrt{\pi}}\left(\int_{\bar{h}(\mathbf{r})}^{\infty} dw\,\mathrm{erfc}[H(w,\mathbf{r},t)]e^{-w^2}\right)\right.$$
$$\left. - P(\mathbf{r})\right], \qquad (33)$$

where

$$H(w,\mathbf{r},t) \equiv \frac{\bar{h}(\mathbf{r}) - A(\mathbf{r},t)w}{\sqrt{1 - A^2(\mathbf{r},t)}}, \qquad (34)$$

and $A(\mathbf{r},t)$ is the normalized autocorrelation function

$$A(\mathbf{r},t) \equiv \frac{\langle h(\mathbf{r},t)h(\mathbf{r},0)\rangle}{\langle h^2(\mathbf{r})\rangle}. \qquad (35)$$

The expressions in Eqs. (31) and (33) allow us to calculate $P(\mathbf{r})C(\mathbf{r},t_D)$, and therefore D_{macro}, solely from knowledge of the time correlation function. We obtain $D_{\mathrm{macro}} = 9.2 \times 10^{-4}\ \mu m^2\ s^{-1}$ which matches the value obtained by FSBD.

However, the experimental result $D_{\mathrm{macro}} = 6.6 \times 10^{-3}\ \mu m^2\ s^{-1}$ [51] is larger, a discrepancy which we attempt to address in the following sections by adding more realistic interactions.

The pinned membrane

As discussed in the protein mobility section, the lipid bilayer is locally pinned to the cytoskeleton at discrete points. A more realistic model than that of the free membrane contains the interaction [33,37]

$$\mathcal{H}_{\mathrm{pin}}(h(\mathbf{r})) = \frac{\gamma}{2}h^2(\mathbf{r})\sum_i\ \exp\left[-\left(\frac{\mathbf{r}-\mathbf{R}_i}{\ell/4}\right)^2\right], \qquad (36)$$

where γ in Table I is sufficiently large that the height is essentially confined to zero near the pinning sites $\mathbf{R}_i$ labeled by the index i. The potential locally acts on an area $\sim\ell^2$ (which is also approximately the cross-sectional area of the anchoring protein). We use in this section the simple pinning geometry of a square grid with pinning sites at every multiple of L.

The pinning of the membrane allows us to increase the system size to large $\mathcal{L}$ so that each individual corral is allowed to have a nonzero center of mass even though the entire system maintains $h_{\mathrm{c.m.}} = 0$. We use a system size of $\mathcal{L} = 4L$ chosen such that our results no longer change with further increases in $\mathcal{L}$. The resulting configurations of the corral are more realistic since we expect that in the real red blood cell, the center of mass of individual corrals will fluctuate. By increasing the system size, we also allow wavelength $\sim 2L$ modes that were not present in the free membrane. Since the longer wavelength modes are dominant, we expect a strong contribution from these modes.

The pinning potential couples the modes in the Hamiltonian and the equations of motion for the amplitudes. A detailed analysis of the diagonalization procedure used to obtain exact results for the time autocorrelation function is given in Brown [33] (with a brief discussion in Appendix A) and a comparison with FSBD is given in Fig. 2. The slower decay of the correlation function reflects the inclusion of the longer wavelength modes discussed above. The results in Ref. [33] combined with the results in Appendix A give the exact result for the position correlation function which is compared to FSBD in Fig. 2. The correlations are positive
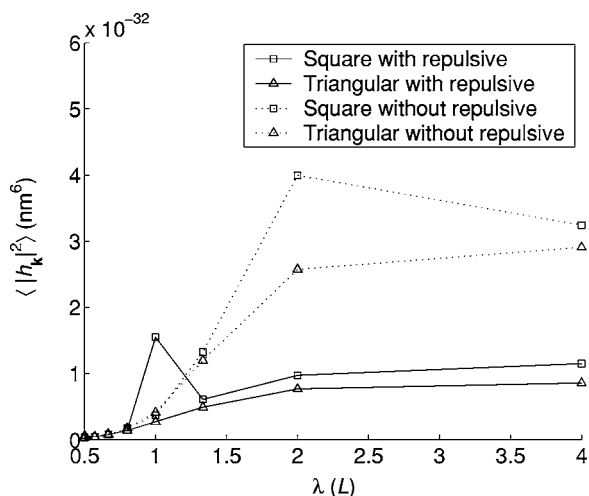
FIG. 4. Plot of the amplitude $\langle |h_{\mathbf{k}}|^2 \rangle$ as a function of the wavelength $\lambda = 2\pi/k$. We have set $n=0$ in the wave vector $\mathbf{k} = (m,n)2\pi/\mathcal{L}$ to study the modes parallel to the edge of the corrals. The system size is $\mathcal{L}=4L$.

over an entire single corral, indicating the dominance of the wavelength $2L$ modes. A plot of the amplitude $\langle |h_{\mathbf{k}}|^2 \rangle$ as a function of the wavelength $\lambda = 2\pi/k$ in Fig. 4 does indeed show a peak at wavelength $\lambda = 2L$.

Knowledge of the time correlation function allows us to compute the macroscopic diffusion constant using the results of the protein mobility section. Comparison with the direct simulation again yields the same results within error as shown in Fig. 5. The value of the macroscopic diffusion constant calculated for this model 7.0×10^{-2} μm^2 s^{-1} is about an order of magnitude larger than the experimental value. The increase in D_{macro} over the free membrane model is a result of the persistence of correlations as shown in Fig. 2 as well as an increase in height fluctuations. Both effects are due to the longer wavelength $\sim 2L$ modes which we later
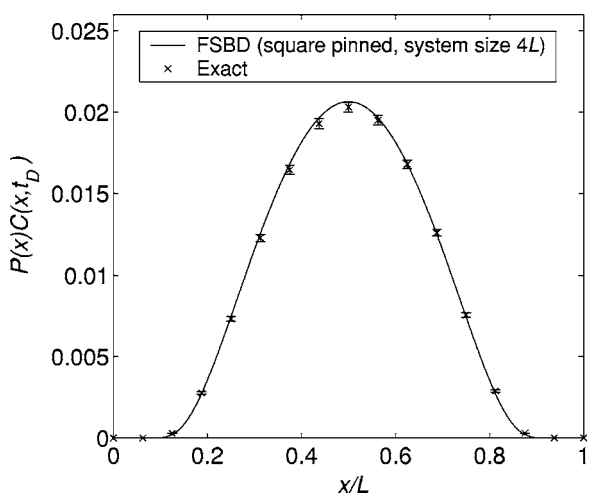

FIG. 5. Plot of $P(x)C(x,t_D)$ along the edge of the corral x for a pinned membrane of system size $\mathcal{L}=4L$ with $L=112$ nm. The parameters used are the same as in Fig. 2. The error bars are calculated from the standard deviation of the mean of 100 samples each consisting of an average over all corral edges for a block of 1 ms.

see are quenched to some extent by the repulsive interaction of the cytoskeleton in our more detailed (anharmonic) simulations.

Nonharmonic interactions

The FSBD algorithm is most useful when applied to systems which cannot be treated analytically. One such system, studied previously by Gouliaev and Nagle [34], is a model which mimics the potential of a stack of membranes. The interaction term used by these authors is given by

$$\mathcal{H}_{\mathrm{wall}}(h(\mathbf{r})) = \tfrac{1}{2}[V(a+h(\mathbf{r})) + V(a-h(\mathbf{r}))], \qquad (37)$$

where $V(z) = A\lambda \exp(-z/\lambda) - H/12\pi z^2$, and A, H, and λ are constants. Hard walls are taken to be located at $z = \pm a$. Here, the physical quantities of interest are the root mean square displacement $h_{\mathrm{rms}} \equiv \sqrt{\overline{h^2}}$ and the pressure P given by [34]

$$P = - \overline{\frac{\partial \mathcal{H}_{\mathrm{wall}}}{\partial a}}, \qquad (38)$$

where the bar indicates an average over space and time. The expression for the pressure reflects noncontact interactions with the wall. For the parameter sets of interest, the pressure due to collisions with the hard wall are negligible [34].

We have verified in previous work [37] that the results from FSBD match those of the Monte Carlo simulations found in Nagle [34]. All of the previously studied cases assume vanishing tension. We extend several of these cases by including a finite surface tension and comparing the results of FSBD with Monte Carlo calculations in Table II. The surface tension is chosen to be the same value $\sigma = (2\pi/\mathcal{L})^2 K_c$ as in the preceding section. As expected, we see a decrease in both the height of the fluctuations and the pressure. It should be noted that the hydrodynamic flows are expected to be confined for a stack of membranes. The correct dynamics are obtained by replacing the Oseen tensor with a modified form incorporating impermeable wall boundary conditions [75–77]. However, static equilibrium properties are completely independent of the hydrodynamic kernel and therefore our use of the usual Oseen tensor for unconfined geometries presents no problems for the calculation of height fluctuations and pressure.

To explain the relatively small drop in h_{rms}, we first note that we have chosen a value of σ such that the bending and surface tension energies are equal for the longest wavelength modes [see Eq. (18)]. Since these modes dominate, the energies of both are approximately equal. We assess the relative importance of the interaction with the wall by comparing h_{rms} with and without the term $\mathcal{H}_{\mathrm{wall}}$. For a membrane with only a bending energy term, the average root mean square height is ~ 10 Å for the first parameter set and ~ 30 Å for the second. Adding the interaction of the wall strongly suppresses fluctuations as can be seen by comparing to Table II. Since $\mathcal{H}_{\mathrm{wall}}$ dominates, the addition of a surface tension with energy on the order of the bending energy does little to further quench undulations. The pressure, however, has a term that depends exponentially on the height. Small changes in $h(\mathbf{r})$ can have a larger effect as seen in Table II.

TABLE II. Comparison between MC and FSBD: The root mean square height h_{rms}(Å) and pressure P(ergs/cm^3) for a membrane confined between two walls using $N=8$, $\mathcal{L}=700$ Å, $T=323$ K, and $A=10^9$ ergs/cm^3. In the nonzero surface tension cases, the value $\sigma = (2\pi/\mathcal{L})^2 K_c$ is used. The Monte Carlo data in the first column ($\sigma=0$) is taken from Gouliaev and Nagle [34] while those of the second column ($\sigma \neq 0$) are from our own Monte Carlo. For the FSBD, a time step of $\Delta t=0.01$ ns was used and the total time of each simulation was $t=1$ ms. The errors are calculated using standard statistical estimates [78,79].

Parameter set	h_{rms} (MC, $\sigma=0$)	h_{rms} (MC, $\sigma \neq 0$)	h_{rms} (FSBD, $\sigma \neq 0$)
(1)	4.3366±0.0013	4.2087±0.0022	4.2031±0.0019
(2)	6.1225±0.0030	6.0868±0.0019	6.0851±0.0017
Parameter set	P (MC, $\sigma=0$)	P (MC, $\sigma \neq 0$)	P (FSBD, $\sigma \neq 0$)
(1)	173470±170	156690±280	156180±170
(2)	38500±1000	26090±640	26240±320

Parameter set (1): $H=0\times10^{-14}$ ergs, $K_c=10^{-12}$ ergs, $\lambda=1.8$Å, $a=20$ Å

Parameter set (2): $H=3\times10^{-14}$ ergs, $K_c=10^{-13}$ ergs, $\lambda=1.4$ Å, $a=17$ Å

REPULSIVE CYTOSKELETAL INTERACTIONS

We return to the problem of protein mobility and consider the addition of a repulsive interaction between the cytoskeleton and the membrane. For this nonharmonic model, our only means of obtaining quantitative results is through the use of the FSBD algorithm. We add to the pinning term $\mathcal{H}_{pin}$ an additional potential due to the cytoskeleton. The repulsive interactions between the spectrin and lipid bilayer are approximated as a short-range hydration potential of the form [73]

$$\mathcal{H}_{rep}(h(\mathbf{r})) = \epsilon \sum_i e^{-h(\mathbf{r})/\lambda} \exp\left[-\left(\frac{a_i x + b_i y + c_i}{\ell/4}\right)^2\right],$$

(39)

where $a_i x + b_i y + c_i = 0$ specifies a particular finite linear segment of spectrin between pinning sites. The potential is restricted to a line of width of $\sim \ell$ (approximately the width of the spectrin). In accordance with experiments on repulsive interactions between membranes [80], the steepness of the potential is taken to be $\lambda=0.2$ nm. The value $\epsilon=k_B T/100\ell^2$ is chosen to force the potential to rise rapidly once $h(\mathbf{r})$ is less than zero.

As a result of the asymmetry of the cytoskeletal repulsion in the z direction, it is unnatural to fix the center of mass at zero. As discussed previously, we choose the value $\Lambda_0 = 3\mathcal{L}/8\pi\eta$ for the dynamics of $h_{c.m.}$. However, by performing the simulation in the limit of large system size $\mathcal{L}$, the center of mass becomes essentially fixed to its natural equilibrium value and the choice of Λ_0 does not affect the results. For $\mathcal{L}\geq 4L$, the results are independent of the system size as seen in Fig. 6. As an additional check, we note that using $\Lambda_0=0$ and $h_{\mathbf{k}=0}$ fixed to the equilibrium value $\langle h_{\mathbf{k}=0}\rangle$ gives results that are indistinguishable within statistical error.

The presence of spectrin filaments below the membrane surface has the potential to alter hydrodynamics inside the cell relative to a membrane suspended in a homogeneous medium. It has been argued that the possible confinement of hydrodynamic flow due to the cytoskeleton might be incorporated through a generalized interaction kernel in Eq. (9) in

lieu of the Oseen tensor [31]. While this approach may be valid over length scales of hundreds of nanometers and longer, we are most interested on dynamics at smaller wavelengths where such an approach seems questionable. Since cytoskeletal filaments occupy a relatively small fraction of the total area beneath the membrane surface, it seems reasonable to neglect their impact on hydrodynamics. Henceforth, we make this assumption and treat the dynamics of the RBC lipid bilayer as though the only effect of spectrin filaments is to modify the energetics of bilayer conformations. Hydrodynamic consequences of the spectrin meshwork are ignored.

We study both the square corral geometry shown in Fig. 7 and the triangular corral geometry in Fig. 8 both with $L = 112$ nm chosen to agree with the experimental confinement length of $L\sim 110$ nm [51]. All simulations were done with a time step of $\Delta t=1$ ns for a total time of $t=0.1$ s. We plot the
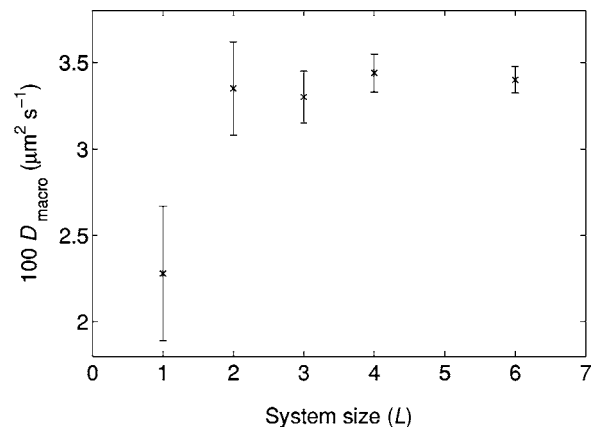

FIG. 6. Plot of the macroscopic diffusion constant as a function of the system size in units of L for the square geometry. The simulations were done with a time step of $\Delta t=1$ ns for a total time of $t=0.1$ s. The error bars are calculated from the standard deviation of the mean of 100 samples each consisting of an average over all corral edges for a block of 1 ms. Since there are more corrals and therefore more independent samples as the system size increases, the error decreases with increasing $\mathcal{L}$.
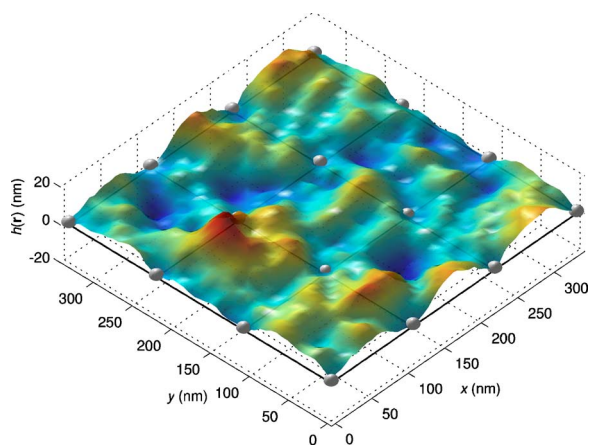
FIG. 7. (Color online) Sample configuration for a membrane ($\mathcal{L}=3L$) with square pinning and cytoskeletal repulsion. The pinning sites are located at every multiple of L and indicated by spheres. The repulsive interaction due to spectrin is localized along the black lines which connect between the pinning sites. The z axis is expanded to help visualize fluctuations in the membrane.

FIG. 9. Plot of the probability that the membrane height exceeds h_0 as a function of the distance x along the edge of the corral for a system size $\mathcal{L}=4L$. The repulsion due to the cytoskeleton pushes the membrane above $h(\mathbf{r})=0$ and therefore increases the probability of opening a gap of size h_0. The error bars for the simulation data are smaller than the symbol size.

equilibrium probability $P(x)$ that the height is greater than h_0 for both the square and triangular geometry in Fig. 9. For comparison, the results for the same systems without the cytoskeletal interactions are also plotted. The repulsive interaction pushes the center of mass above zero and thus increases the probability that the height is greater than h_0. In Fig. 10, we plot $C(t)$ for the same systems.

The addition of the cytoskeleton increases the relaxation rate of height fluctuations, a fact attributed to the suppression of the wavelength $2L$ modes. These modes are quenched since the membrane must stay above $h(\mathbf{r})=0$ at the corral edges while being pinned at every multiple of L. This condition is difficult to satisfy for wavelengths longer than L. To verify this hypothesis, we study the amplitudes of the modes that run in a direction parallel to the corral edges in the x
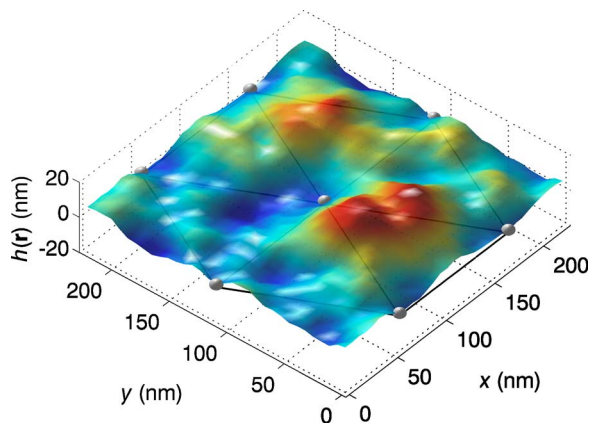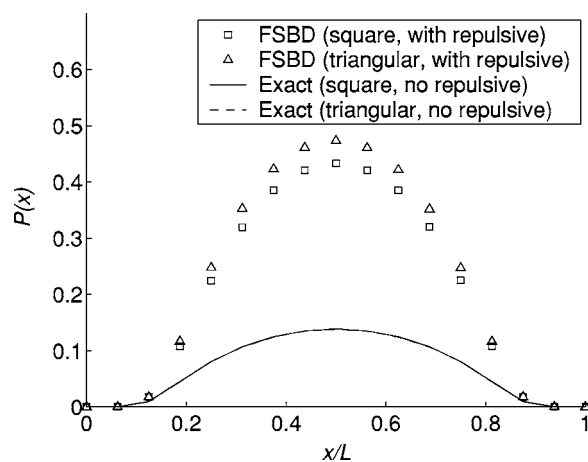
direction. For the square corral geometry, a plot of the amplitudes in Fig. 4 reveals a peak for modes of wavelength L, showing that the longer-lived wavelength $2L$ modes no longer dominate. With pinning sites spaced every L and repulsions acting in between, the square corral geometry forces the membrane to adopt (on average) a configuration that has period L in the x (and y) direction. Troughs occur at the pinning sites with intermediate peaks induced by the cytoskeletal repulsion. In the absence of cytoskeletal repulsions, period L modes hold no special dominance (Fig. 4). In the case of the triangular corral geometry, the wavelength L modes are suppressed. A wavelength L mode running parallel to the base of a triangular corral that is pinned at all corners must have a maximum at the center of the corral edge. This maximum, however, is energetically unfavorable given the
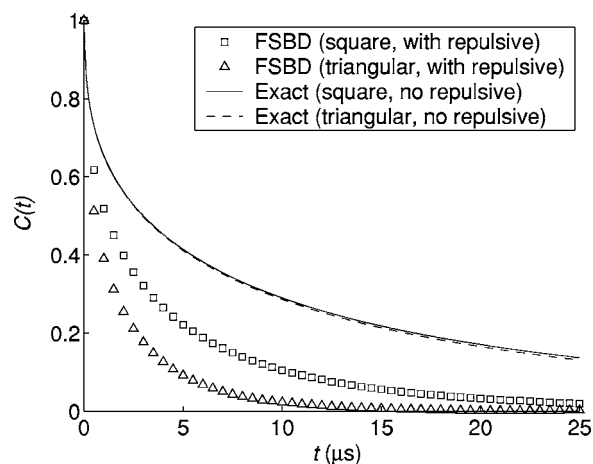

FIG. 8. (Color online) Sample configuration for a membrane ($\mathcal{L}=2L$) with triangular pinning and cytoskeletal repulsion. The pinning sites are located at $(1/2,0)$, $(3/2,0)$, $(1,0)$, $(1,1)$, $(1,2)$, $(2,1/2)$, and $(2,3/2)$ in units of L and are indicated by spheres. The repulsive interaction due to the spectrin is localized along the black lines which connect between the pinning sites. The z axis is expanded to help visualize fluctuations in the membrane.

FIG. 10. Plot of $C(t)$ for $x=L/2$ for a system size $\mathcal{L}=4L$. The amplitudes of the longer-lived wavelength $2L$ modes are quenched by the cytoskeletal repulsion and $C(t)$ mostly reflects the wavelength L modes. The error bars for the simulation data are smaller than the symbol size.
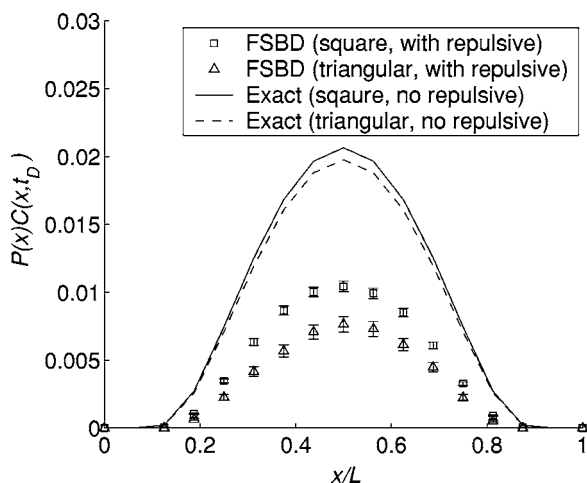
FIG. 11. Plot of $P(x)C(x,t_D)$ as a function of the distance x along the edge of the corral for a system size $\mathcal{L}=4L$. Error bars are calculated from the standard deviation of the mean of 100 samples each consisting of an average over all corral edges for a block of 1 ms.

FIG. 12. Plot of D_{macro} as a function of the height of the cytoplasmic domain of the diffusing protein, h_0, for a membrane with a square pinning geometry and repulsive cytoskeletal interactions.

pinning site at the tip of the triangle above the base. The wavelength L modes do not fit as naturally into the triangular pinning geometry as they do for the square geometry. A peak at L in Fig. 4 is not expected for the triangular geometry, and none is observed.

The product $P(x)C(x,t_D)$ is shown in Fig. 11. Although the membrane has a larger probability of being above h_0 at the edge of the corral, these gaps are short-lived, as discussed above. The overall effect is a reduction in the escape probability and thus the macroscopic diffusion constant. We compare the results in this study against those of the case without the cytoskeletal repulsion of our previous study [33]. For the square geometry, $D_{\mathrm{macro}}=(3.44\pm0.11)\times10^{-2}~\mu\mathrm{m}^2~\mathrm{s}^{-1}$ compared to $D_{\mathrm{macro}}=7.0\times10^{-2}~\mu\mathrm{m}^2~\mathrm{s}^{-1}$ in the absence of repulsive interactions while for the triangular geometry, $D_{\mathrm{macro}}=(2.06\pm0.13)\times10^{-2}~\mu\mathrm{m}^2~\mathrm{s}^{-1}$ compared to $D_{\mathrm{macro}}=6.6\times10^{-2}~\mu\mathrm{m}^2~\mathrm{s}^{-1}$ in the absence of repulsive interactions.

The values obtained from this model are still ~3 to 5 times larger than the experimentally observed value of $D_{\mathrm{macro}}=6.6\times10^{-3}~\mu\mathrm{m}^2~\mathrm{s}^{-1}$ [51]. The discrepancy is perhaps a result of several approximations in our theoretical treatment. All interactions with the protein are neglected except the one between band 3 and spectrin approximated by the requirement of an opening in the membrane of size h_0 at time 0 and t_D. The cytoskeleton in our model is also completely static. We have ignored the opening of gaps by spectrin dissociation at the corral edge, a mechanism that has been studied elsewhere [54–58]. Other forms of cytoskeletal motion, such as thermal fluctuations of the spectrin filaments [81], have also been ignored.

Mathematically, our estimation of the escape probability proceeds via calculation of $P(\mathbf{r})C(\mathbf{r},t)$, the correlated probability that the height of the membrane is greater than h_0 at both times 0 and t_D. Historically, we chose to study the quantity $P(\mathbf{r})C(\mathbf{r},t)$ because analytical expressions could be obtained for cases involving harmonic potentials [29,33]. Using FSBD simulations, it is also possible to numerically evaluate
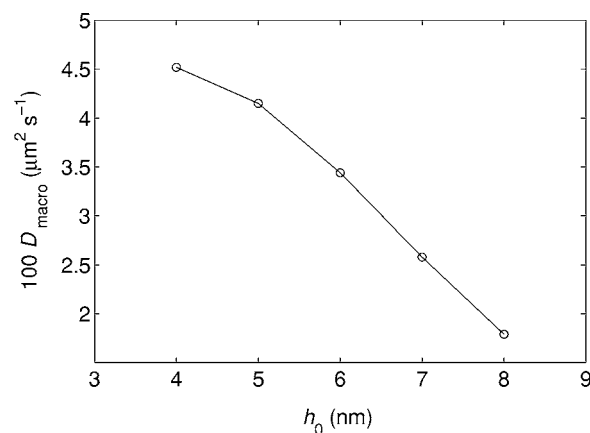
the probability, $P_{\mathrm{open}}(\mathbf{r},t)$, that the height of the membrane exceeds h_0 for the entire time interval $[0,t_D]$. The resulting value of the macroscopic diffusion constant in this case is $D_{\mathrm{macro}}=3.0\times10^{-3}~\mu\mathrm{m}^2~\mathrm{s}^{-1}$ for the square pinning geometry with repulsive cytoskeletal interactions. This value is approximately a factor of 10 smaller than that obtained via the $P(\mathbf{r})C(\mathbf{r},t)$ calculation. Requiring the membrane to remain higher than h_0 for the duration of the diffusive escape event is a stricter condition than that imposed by the correlated probability [29]. The probability for an "opening" event to take place drops in this approximation as does D_{macro}.

We emphasize that both $P(\mathbf{r})C(\mathbf{r},t)$ and $P_{\mathrm{open}}(\mathbf{r},t)$ gating calculations are approximations that we use in lieu of a model with realistic potentials acting between the protein, cytoskeleton, and membrane. We lack detailed knowledge of these potentials and it is thus impossible to guess which model is most appropriate. For simplicity and consistency with prior work, we have presented the results of this paper exclusively in terms of $P(\mathbf{r})C(\mathbf{r},t)$ calculations. Interestingly, the experimental value of the macroscopic diffusion constant lies between the values predicted from the two methods of calculation.

We discuss briefly the dependence of the macroscopic diffusion constant to the parameters in our model. The value of D_{macro} varies between $(4.5-1.8)\times10^{-2}~\mu\mathrm{m}^2~\mathrm{s}^{-1}$ for h_0 between $(4-8)$ nm for the square geometry (see Fig. 12). The sensitivity here is less than in the case without repulsion where the variation is $(17-2.5)\times10^{-2}~\mu\mathrm{m}^2~\mathrm{s}^{-1}$ in the same range of h_0 [33]. Although $h_0=6$ nm is firmly established for the band 3 proteins studied experimentally, this height dependence of diffusion is an experimentally testable prediction of our model. The bending rigidity of the bilayer can also be modified. If we double the value of K_c, the macroscopic diffusion constant decreases by an order of magnitude to $2.2\times10^{-3}~\mu\mathrm{m}^2~\mathrm{s}^{-1}$. Given that the observed value of the bending rigidity may be artificially low due to metabolic processes in the red blood cell acting at long wavelengths [82–84], it is possible that a larger value for K_c is more appropriate, which would bring D_{macro} from the simulation closer to the experimentally observed value.

We have also assumed constant values of several parameters that in general depend on other factors. Although the bending rigidity K_c is expected to vary near the protein and the pinning sites, we use a constant value over the entire membrane. Similarly, the value of the microscopic diffusion constant D is taken to be constant even though it is expected to vary in the presence of other proteins as well as the pinning sites. However, these effects are built into the the experimental values of K_c and D that we employ in an averaged sense.

It should also be noted that metabolic processes in the red blood cell are expected to affect membrane height fluctuations [82–84]. However, the bending rigidity is measured in the presence of this activity and the value of K_c incorporates these effects, albeit in an approximate way. In other words, the values we have used for the elastic constants in this study reflect the amplitude of undulations observed under physiological conditions where energy is being expended by the cell. The use of such effective parameters within a framework of thermal equilibrium fluctuations is clearly a severe approximation, yet has a long history of success in explaining red blood cell dynamics. Incorporating realistic nonthermal energy sources within an elastic membrane model is of interest and may eventually lead to a more satisfactory understanding of the red cell membrane than the phenomenological approach considered here.

A further consideration is the irregularity of the corral shapes and sizes in the red blood cell. The single particle tracking experiments done by Tomishige *et al.* [51] show that the corral sizes vary from 50 to 200 nm and that the macroscopic diffusion constant can vary from 10^1 to 10^{-3} $\mu m^2 s^{-1}$. The experimental values we have quoted within this work for both L and D_{macro} are the median values. The large variation in experimental data could also account for some of the discrepancy between experiment and modeling. Despite the approximations listed above, our results clearly indicate that membrane fluctuations likely play a role in the global diffusion of band 3 on the red blood cell. At the very least, it is not possible to ignore such dynamics a priori as has previously been assumed.

CONCLUSION

We have introduced a Fourier space Brownian dynamics simulation method that allows for the time evolution of lipid bilayers over long length and time scales. The algorithm is general enough to handle arbitrary interactions between membrane and environment and should therefore be useful for studying many processes inaccessible to more detailed simulations. We have verified the accuracy of FSBD by comparing to several cases for which exact answers are available. These cases include dynamical quantities for harmonic interactions and equilibrium quantities for nonharmonic interactions. The FSBD algorithm, however, goes further by treating the dynamics of nonharmonic systems. Our method is quite general, with potential applications to a wide variety of biophysical processes including fluctuations of supported bilayers [85], nonthermal shape fluctuations of vesicles [86,87], and polymerization of cytoskeletal filaments against

membrane surfaces [88]. We are currently pursuing these and related questions.

We have exploited the generality of FSBD in our examination of the effects of thermal membrane undulations on protein mobility. Past studies [29,33] considered free membranes and membranes pinned at localized sites to the underlying cytoskeleton. As an improvement, we considered a repulsive potential between the bilayer and spectrin filaments while keeping the localized pinning sites. This model more accurately reflects the physical situation and dynamics can only be treated by the FSBD method due to the nonharmonic nature of the interaction.

In this model, the repulsive forces push the membrane above the plane at the corral edges and restrict the set of energetically favorable configurations. The modes of wavelength $2L$ are suppressed beyond that of the model containing only pinning sites, a result that is expected based on the fact that these modes cannot simultaneously satisfy both the pinning condition and the repulsion at the corral edges. While the wavelength L modes dominate in the square pinning geometry, these are further suppressed in the triangular system where they do not naturally fit. In the end, we find that the macroscopic diffusion constant predicted by our model is several times larger than the experimental value. The discrepancy is due to the various simplifications in our treatment discussed in the preceding section. However, we believe that the qualitative implications of our study are unambiguous. Thermal membrane undulations are likely a contributing factor and a possible mechanism for the macroscopic diffusion of the proteins on the surface of the red blood cell.

One prediction of this model that seems amenable to experimental verification is the increase of the macroscopic diffusion constant with decreasing height of protein cytoplasmic domain, h_0. In principle, different proteins could be studied and/or proteins engineered with smaller or larger cytoplasmic domains. Experiments do show that D_{macro} increases after cleaving the entire cytoplasmic domain of the protein [51], but we are unaware of any systematic studies of diffusion with varying h_0. Other seemingly "verifiable" predictions (temperature dependence, viscosity dependence, K_c dependence, etc.) are not anticipated to be captured correctly within the simple picture presented here. Changing temperature will lead to biochemical changes not anticipated by our model that may influence other physical properties. Altering K_c and/or cytoplasm viscosity will require chemical changes that are also likely to affect this complex system in unpredictable ways.

ACKNOWLEDGMENTS

APPENDIX A: HEIGHT CORRELATIONS

We compute height correlations in space and time in Fourier space

$$\langle h(\mathbf{r},t)h(\mathbf{r}',t')\rangle = \frac{1}{\mathcal{L}^4}\sum_{\mathbf{k}\mathbf{k}'}\langle h_{\mathbf{k}}(t)h_{\mathbf{k}'}(t')\rangle e^{i\mathbf{k}\cdot\mathbf{r}+i\mathbf{k}'\cdot\mathbf{r}'}. \quad \text{(A1)}$$

The height $h(\mathbf{r})$ is real, and therefore the amplitudes obey the relation $h_{\mathbf{k}}^* = h_{-\mathbf{k}}$ which we use to simplify the expression

$$\langle h(\mathbf{r},t)h(\mathbf{r}',t')\rangle = \frac{1}{\mathcal{L}^4}\sum_{\mathbf{k}\mathbf{k}'}\langle H(\mathbf{k},\mathbf{r},t)H(\mathbf{k}',\mathbf{r}',t')\rangle, \quad \text{(A2)}$$

where we have defined $H(\mathbf{k},\mathbf{r},t) \equiv a_{\mathbf{k}}(t)\cos\mathbf{k}\cdot\mathbf{r} - b_{\mathbf{k}}(t)\sin\mathbf{k}\cdot\mathbf{r}$ and $h_{\mathbf{k}} = a_{\mathbf{k}} + ib_{\mathbf{k}}$. Computing the correlation functions is equivalent to computing the correlations between the real and imaginary parts of the amplitude $h_{\mathbf{k}}$.

The free membrane model decouples in Fourier space and is equivalent to an Ornstein-Uhlenbeck process for each mode [29]. The correlation functions are

$$\langle a_{\mathbf{k}}(t)a_{\mathbf{k}'}(t')\rangle = \frac{k_B T \mathcal{L}^2 e^{-\omega_{\mathbf{k}}|t-t'|}}{2K_c k^4}(\delta_{\mathbf{k},\mathbf{k}'} + \delta_{\mathbf{k},-\mathbf{k}'}) \quad \text{(A3)}$$

and similarly for the imaginary parts with correlations between real and imaginary components equal to zero. Using the above, we recover Eq. (27).

For the pinned membrane, the modes become coupled. Using a diagonalization procedure, the eigenmodes are once again Ornstein-Uhlenbeck processes [33] and the correlations in amplitude become

$$\langle c_{\mathbf{q}}(t)c_{\mathbf{q}'}(t')\rangle = \sqrt{\Lambda_{\mathbf{q}}\Lambda_{\mathbf{q}'}}\sum_i \frac{\mathcal{L}}{2\beta\omega_i}U_{\mathbf{q}i}U_{\mathbf{q}'i}e^{-\omega_i t}, \quad \text{(A4)}$$

where $\mathbf{q}$ label only the independent modes (since the $\mathbf{k}$ mode is equivalent to the $-\mathbf{k}$ mode), $c_{\mathbf{q}}$ is a vector of the modes $(\{a_{\mathbf{q}}\},\{b_{\mathbf{q}}\})$, the eigenmodes are labeled by the index i, and ω_i and $U_{\mathbf{q}i}$ are the eigenvalues and eigenvectors, respectively, of the matrix (A11) defined in Ref. [33]. Once the correlations between all amplitudes are known, the full correlation function follows by plugging into Eq. (A2).

APPENDIX B: TIME STEP ESTIMATES

We show for the free membrane that the value of the time step chosen is reasonable, although for more complicated cases, we reduce the time step until the results stabilize within error bars. The treatment here closely follows that of Schulten and Kosztin [89]. The equation of motion for each of the modes for the free membrane is

$$\dot{h}_{\mathbf{k}} = -\omega_{\mathbf{k}}h_{\mathbf{k}} + \zeta_{\mathbf{k}}. \quad \text{(B1)}$$

We define $h_{\mathbf{k}} \equiv a_{\mathbf{k}} + ib_{\mathbf{k}}$, and use Eq. (26) and the width of $R(\Delta t) \sim \mathcal{L}^2 k_B T \Lambda_{\mathbf{k}}\Delta t$ to obtain the form of the equation of motion for the real part of each mode (and similarly for the imaginary part)

$$\Delta a_{\mathbf{k}} = A\Delta t + B\sqrt{\Delta t}, \quad \text{(B2)}$$

where

$$A = \omega_{\mathbf{k}}a_{\mathbf{k}}^0 = \omega_{\mathbf{k}}\sqrt{\langle a_{\mathbf{k}}^2\rangle},$$

$$\text{(B3)}$$

$$B = \sqrt{\mathcal{L}^2 k_B T \Lambda_{\mathbf{k}}}.$$

We have taken the initial amplitude $a_{\mathbf{k}}^0$ and also B to be typical values one standard deviation from the mean. Solving for the time step, we obtain

$$\Delta t = \frac{1}{2A^2}(B^2 + 2A\Delta a_{\mathbf{k}} - B\sqrt{B^2 + 4A\Delta a_{\mathbf{k}}}), \quad \text{(B4)}$$

where the value of $\Delta a_{\mathbf{k}}$ is determined by the accuracy desired in the linear approximation of the equation of motion. The energy of each mode is

$$V(a_{\mathbf{k}}) = \frac{K_c k^4}{L^2}a_{\mathbf{k}}^2 \quad \text{(B5)}$$

and the change in energy over the time step in the linear approximation is

$$\Delta V(a_{\mathbf{k}}) = V(a_{\mathbf{k}}^0 + \Delta a_{\mathbf{k}}) - V(a_{\mathbf{k}}^0) - \frac{dV(a_{\mathbf{k}}^0)}{da_{\mathbf{k}}}\Delta a_{\mathbf{k}}, \quad \text{(B6)}$$

which leads to

$$\Delta a_{\mathbf{k}} = \sqrt{\frac{\Delta V(a_{\mathbf{k}})\mathcal{L}^2}{K_c k^4}}. \quad \text{(B7)}$$

A value of $\Delta V(a_{\mathbf{k}}) = 0.1 k_B T$ gives for the largest and smallest wave vector,

$$\Delta t = 0.3 \text{ ns} \quad \text{for} \quad \mathbf{k} = \frac{2\pi}{\mathcal{L}}(8,8), \quad \text{(B8)}$$

$$\Delta t = 500 \text{ ns} \quad \text{for} \quad \mathbf{k} = \frac{2\pi}{\mathcal{L}}(1,0). \quad \text{(B9)}$$

The Hamiltonian and the equations of motion show that the long wavelength modes dominate in the quantities that we compute. The value $\Delta t = 1$ ns is reasonable given the agreement between the analytical results and the simulation.

If the membrane is locally pinned with the potential

$$V = \frac{\gamma\ell^2}{2}h^2 \quad \text{(B10)}$$

and we assume that this area is a sphere of radius $\ell/2$ undergoing diffusion with the drag force given by Stokes' law, then the Langevin equation is

$$\dot{h}(t) = \frac{1}{3\pi\eta\ell}[-\gamma\ell^2 h(t) + f(t)], \quad \text{(B11)}$$

where

$$\langle f(t)f(t')\rangle = 2k_B T(3\pi\eta\ell)\delta(t-t'). \quad \text{(B12)}$$

Using the same equations as for the free membrane

$$A = \frac{\gamma\ell^2\sqrt{\langle h^2\rangle}}{3\pi\eta\ell}, \quad \text{(B13)}$$

$$B = \sqrt{\frac{2k_BT}{3\pi\eta\ell}},$$

where

$$\sqrt{\langle h^2 \rangle} = \sqrt{\frac{k_BT}{\gamma\ell^2}}. \tag{B14}$$

Using $\Delta V = 0.1 k_B T$, we get a time step of $\Delta t = 0.3$ ns. We find, however, that $\Delta t = 1$ ns is adequate as indicated by the agreement with the analytical results in Fig. 2.

---

[1] S. E. Feller, Curr. Opin. Colloid Interface Sci. **5**, 217 (2000).

[2] R. W. Pastor, Curr. Opin. Struct. Biol. **4**, 486 (1994).

[3] D. J. Tobias, K. C. Tu, and M. L. Klein, Curr. Opin. Colloid Interface Sci. **2**, 15 (1997).

[4] S. J. M. D. P. Tieleman and H. J. C. Berendsen, Biochim. Biophys. Acta **1331**, 235 (1997).

[5] S. J. Marrink, E. Lindahl, O. Edholm, and A. E. Mark, J. Am. Chem. Soc. **123**, 8638 (2001).

[6] J. Shillcock and R. Lipowsky, J. Chem. Phys. **117**, 468 (2002).

[7] S. Yamamoto, Y. Maruyama, and S. aki Hyodo, J. Chem. Phys. **116**, 5842 (2002).

[8] C. F. Lopez, P. B. Moore, J. C. Shelley, M. Y. Shelley, and M. L. Klein, Comput. Phys. Commun. **147**, 1 (2002).

[9] B. Smit, K. Esselink, P. Hilbers, N. van Os, L. Rupert, and I. Szleifer, Langmuir **9**, 9 (1993).

[10] R. D. Groot and K. L. Rabone, Biophys. J. **81**, 725 (2001).

[11] R. Goetz and R. Lipowsky, J. Chem. Phys. **108**, 7397 (1998).

[12] T. Soddemann, B. Dunweg, and K. Kremer, Eur. Phys. J. E **6**, 409 (2001).

[13] G. Ayton, S. G. Bardenhagen, P. McMurty, D. Sulsky, and G. A. Voth, J. Chem. Phys. **114**, 6913 (2001).

[14] J.-M. Drouffe, A. C. Maggs, and S. Leibler, Science **254**, 1353 (1991).

[15] H. Noguchi and M. Takasu, J. Chem. Phys. **115**, 9547 (2001).

[16] O. Farago, J. Chem. Phys. **119**, 596 (2003).

[17] G. Brannigan and F. L. H. Brown, J. Chem. Phys. **120**, 1059 (2004).

[18] W. Helfrich, Z. Naturforsch. C **28**, 693 (1973).

[19] F. Brochard and J. F. Lennon, J. Phys. (Paris) **36**, 1035 (1975).

[20] N. Dan, P. Pincus, and S. A. Safran, Langmuir **9**, 2768 (1993).

[21] M. Goulian, R. Bruinsma, and P. Pincus, Europhys. Lett. **22**, 145 (1993).

[22] K. S. Kim, J. Neu, and G. Oster, Biophys. J. **75**, 2274 (1998).

[23] R. Golestanian, M. Goulian, and M. Kardar, Phys. Rev. E **54**, 6725 (1996).

[24] T. R. Weikl, Phys. Rev. E **66**, 061915 (2002).

[25] S. Y. Qi, J. T. Groves, and A. K. Chakraborty, Proc. Natl. Acad. Sci. U.S.A. **98**, 6548 (2001).

[26] S. T. Milner and S. A. Safran, Phys. Rev. A **36**, 4371 (1987).

[27] M. B. Schneider, J. T. Jenkins, and W. W. Webb, J. Phys. (Paris) **45**, 1457 (1984).

[28] R. Granek, J. Phys. II **7**, 1761 (1997).

[29] F. L. H. Brown, Biophys. J. **84**, 842 (2003).

[30] R. Granek and J. Klafter, Europhys. Lett. **56**, 15 (2001).

[31] N. Gov, A. G. Zilman, and S. Safran, Phys. Rev. Lett. **90**, 228101 (2003).

[32] N. Gov and S. A. Safran, Phys. Rev. E **69**, 011101 (2004).

[33] L. C.-L. Lin and F. L. H. Brown, Biophys. J. **86**, 764 (2004).

[34] N. Gouliaev and J. F. Nagle, Phys. Rev. E **58**, 881 (1998).

[35] N. Gouliaev and J. F. Nagle, Phys. Rev. Lett. **81**, 2610 (1998).

[36] T. R. Weikl and R. Lipowsky, Langmuir **16**, 9338 (2000).

[37] Lawrence C.-L. Lin and F. L. H. Brown, Phys. Rev. Lett. **93**, 256001 (2004).

[38] R. J. Cherry, Biochim. Biophys. Acta **559**, 289 (1979).

[39] M. Schindler, D. E. Koppel, and M. P. Sheetz, Proc. Natl. Acad. Sci. U.S.A. **77**, 1457 (1980).

[40] M. P. Sheetz, M. Schindler, and D. E. Koppel, Nature (London) **285**, 510 (1980).

[41] D. E. Koppel, M. P. Sheetz, and M. Schindler, Proc. Natl. Acad. Sci. U.S.A. **78**, 3576 (1981).

[42] M. P. Sheetz, Semin Hematol. **20**, 175 (1983).

[43] S. J. Singer and G. L. Nicolson, Science **175**, 720 (1972).

[44] P. G. Saffman and M. Delbruck, Proc. Natl. Acad. Sci. U.S.A. **73**, 3111 (1975).

[45] A. Tsuji and S. Ohnishi, Biochemistry **25**, 6133 (1986).

[46] A. Tsuji, K. Kawasaki, S. Ohnishi, H. Merkle, and A. Kusumi, Biochemistry **27**, 7447 (1988).

[47] M. Edidin, S. C. Kuo, and M. P. Sheetz, Science **254**, 1379 (1991).

[48] J. D. Corbett, P. Agre, J. Palek, and D. E. Golan, J. Clin. Invest. **94**, 683 (1994).

[49] A. Kusumi and Y. Sako, Curr. Opin. Cell Biol. **8**, 566 (1996).

[50] M. Tomishige, Ph.D. thesis, The University of Tokyo, 1997.

[51] M. Tomishige, Y. Sako, and A. Kusumi, J. Cell Biol. **142**, 989 (1998).

[52] A. Kusumi, Y. Sako, and M. Yamamoto, Biophys. J. **65**, 2021 (1993).

[53] M. J. Saxton, Biophys. J. **69**, 389 (1995).

[54] M. J. Saxton, Biophys. J. **55**, 21 (1989).

[55] M. J. Saxton, Biophys. J. **57**, 1167 (1990).

[56] M. J. Saxton, Int. J. Biochem. **22**, 801 (1990).

[57] D. M. Leitner, F. L. H. Brown, and K. R. Wilson, Biophys. J. **78**, 125 (2000).

[58] F. L. H. Brown, D. M. Leitner, J. A. McCammon, and K. R. Wilson, Biophys. J. **78**, 2257 (2000).

[59] T. J. Byers and D. Branton, Proc. Natl. Acad. Sci. U.S.A. **82**, 6153 (1985).

[60] S. Liu, L. Derick, and J. Palek, J. Cell Biol. **104**, 527 (1987).

[61] E. J. Luna and A. L. Hitt, Science **258**, 955 (1992).

[62] T. L. Steck, in *Cell Shape: Determinants, Regulation and Regulatory Role*, edited by W. Stein and F. Bronner (Academic, New York, 1989), pp. 205–246.

[63] P. Jamney, *Structure and Dynamics of Membranes: Part A From Cells to Vesicles* (Elsevier Science, Amsterdam, 1995), pp. 805–849.

[64] E. Sackmann, *Structure and Dynamics of Membranes: Part A. From Cells to Vesicles* (Elsevier Science, Amsterdam, 1995), pp. 1–62.

[65] D. Zhang, A. Klyatkin, J. T. Bolin, and P. S. Low, Blood **96**, 2925 (2000).

[66] S. A. Safran, *Statistical Thermodynamics of Surfaces, Interfaces and Membranes* (Westview Press, Boulder, CO, 1994).

[67] R. Goetz, G. Gompper, and R. Lipowsky, Phys. Rev. Lett. **82**, 221 (1999).

[68] E. Lindahl and O. Edholm, Biophys. J. **79**, 426 (2000).

[69] S. J. Marrink and A. E. Mark, J. Phys. Chem. B **105**, 6122 (2001).

[70] M. Doi and S. F. Edwards, *The Theory of Polymer Dynamics* (Clarendon, Oxford, 1986).

[71] N. G. van Kampen, *Stochastic Processes in Physics and Chemistry* (North-Holland, Amsterdam, 1992), pp. 63,83,220–221.

[72] D. L. Ermak and J. A. McCammon, J. Chem. Phys. **69**, 1352 (1978).

[73] R. Podgornik and V. A. Parsegian, Langmuir **8**, 557 (1992).

[74] J.-B. Fournier, D. Lacoste, and E. Raphael, Phys. Rev. Lett. **92**, 018102 (2004).

[75] U. Seifert, Phys. Rev. E **49**, 3124 (1994).

[76] J. Prost, J.-B. Manneville, and R. Bruinsma, Eur. Phys. J. B **1**, 465 (1998).

[77] N. Gov, A. G. Zilman, and S. Safran, Phys. Rev. E **70**, 011104 (2004).

[78] R. Zwanzig and N. K. Ailawadi, Phys. Rev. **182**, 280 (1969).

[79] D. Frenkel and B. Smit, *Understanding Molecular Simulation*, 2nd ed. (Academic, San Diego, 2002), pp. 525–532.

[80] K. Gawrisch, D. Ruston, J. Zimmerberg, V. A. Parsegian, R. P. Rand, and N. Fuller, Biophys. J. **61**, 1213 (1992).

[81] D. H. Boal and S. K. Boey, Biophys. J. **69**, 372 (1995).

[82] S. Tuvia, A. Almagor, A. Bitler, S. Levin, R. Korenstein, and S. Yedgar, Proc. Natl. Acad. Sci. U.S.A. **94**, 5045 (1997).

[83] S. Tuvia, S. Levin, A. Bitler, and R. Korenstein, J. Cell Biol. **141**, 1551 (1998).

[84] N. Gov and S. A. Safran, Biophys. J. **88**, 1859 (2005).

[85] Y. Kaizuka and J. T. Groves, Biophys. J. **86**, 905 (2004).

[86] J.-B. Manneville, P. Bassereau, D. Levy, and J. Prost, Phys. Rev. Lett. **82**, 4356 (1999).

[87] J.-B. Manneville, P. Bassereau, S. Ramaswamy, and J. Prost, Phys. Rev. E **64**, 021908 (2001).

[88] D. K. Fygenson, J. F. Marko, and A. Libchaber, Phys. Rev. Lett. **79**, 4497 (1997).

[89] K. Schulten and I. Kosztin, Lectures in Theoretical Biophysics, 2000, http://www.ks.uiuc.edu/Services/Class/NSM.pdf